Cofactor-independent pinacolase directs non-Diels-Alderase biogenesis of the Brevianamides

Ying Ye,[1#] Lei Du,[2,3#] Xingwang Zhang,[2,4] Sean A. Newmister,[1] Morgan McCauley,[5] Juan V. Alegre-Requena,[5] Wei Zhang,[2] Shuai Mu,[6] Atsushi Minami,[7] Amy E. Fraley,[1] Maria L. Adrover-Castellano,[1] Nolan A. Carney,[1] Vikram V. Shende,[1] Feifei Qi,[3] Hideaki Oikawa,[7] Hikaru Kato,[8] Sachiko Tsukamoto,[8] Robert S. Paton,[5,9] Robert M. Williams,[5,10*] David H. Sherman,[1,11*] and Shengying Li[2,3,4*]

[1]Life Sciences Institute, University of Michigan, Ann Arbor, Michigan 48109, USA

[2]State Key Laboratory of Microbial Technology, Shandong University, Qingdao, Shandong, 266237, China

[3]Shandong Provincial Key Laboratory of Synthetic Biology, CAS Key Laboratory of Biofuels, Qingdao Institute of Bioenergy and Bioprocess Technology, Chinese Academy of Sciences, Qingdao, Shandong, 266101, China

[4]Laboratory for Marine Biology and Biotechnology, Qingdao National Laboratory for Marine Science and Technology, Qingdao, Shandong 266237, China

[5]Department of Chemistry, Colorado State University, Fort Collins, Colorado 80523, USA

[6]Tianjin Institute of Pharmaceutical Research, Tianjin, 300193, China

[7]Department of Chemistry, Faculty of Science, Hokkaido University, Sapporo 060-0810, Japan

[8]Graduate School of Pharmaceutical Sciences, Kumamoto University, 5-1 Oe-honmachi, Kumamoto 862-0973, Japan

[9]Chemical Research Laboratory, University of Oxford, Mansfield Road, Oxford, OX1 3TA, UK

[10]University of Colorado Cancer Center, Aurora, CO 80045, USA

[11]Departments of Medicinal Chemistry, Chemistry and Microbiology & Immunology, University of Michigan, Ann Arbor, MI, USA

[#] These authors contributed equally.

[*]Shengying Li: lishengying@sdu.edu.cn

[*]David H. Sherman: davidhs@umich.edu

[*]Robert M. Williams: robert.williams@colostate.edu

Fungal bicyclo[2.2.2]diazaoctane indole alkaloids represent an important family of natural products with a wide-spectrum of biological activities. Although biomimetic total syntheses have been completed for representative compounds, the details of their biogenesis, especially the mechanisms for assembly of diastereomerically distinct and enantiomerically antipodal metabolites, have remained largely uncharacterized. Brevianamide A represents the most basic form of the sub-family bearing a dioxopiperazine core and a rare 3-*spiro*-ψ-indoxyl skeleton. Here, we identified the Brevianamide A biosynthetic gene cluster from *Penicillium brevicompactum* NRRL 864 and fully elucidated the metabolic pathway by gene disruption, heterologous expression, precursor incorporation experiments, and *in vitro* biochemical analysis. In particular, we determined BvnE as a cofactor-independent isomerase/pinacolase that is essential for selective production of Brevianamide A. Structural elucidation, molecular modeling, and mutational analysis of BvnE, and quantum chemical calculations provided critical mechanistic insights into the diastereoselective formation of the 3-*spiro*-ψ-indoxyl moiety in Brevianamide A. This occurs through a BvnE-controlled semi-pinacol rearrangement and a subsequent spontaneous intramolecular [4+2] *hetero*-Diels-Alder cycloaddition. Resolution of this 50-year old mechanistic mystery together with our recent characterization of the Diels-Alderase-mediated biogenesis of monooxopiperazines highlight the diversified biosynthetic strategies deployed by fungi for creating structurally diverse *spiro*-cyclized indole alkaloids.

Fungal indole alkaloids bearing the unusual bicyclo[2.2.2]diazaoctane core have drawn considerable attention from natural product, synthetic and biological chemists for decades. A wealth of studies on the discovery of analogs (including semi-synthetic, synthetic and natural), biological activities and biosynthetic mechanisms have been conducted.[1] The prominent representatives of this structural family have been recognized by our laboratories and others as belonging to two main biogenetic subfamilies (Fig. 1a): (1) the dioxopiperazines that includes: the insecticidal Brevianamide A and B (**BA**/**BB**) from *Penicillium brevicompactum*,[2] the anticancer agents (-)-Notoamide A isolated from *Aspergillus protuberus* (formerly *Aspergillus* sp. MF297-2), and (+)-Notoamide A from *A. amoenus* (formerly *A. versicolor* NRRL 35600), the anti-cancer agents Stephacidins A and B from *A. ochraceus*, the Sclerotiamides, Versicolamides, Taichunamides, anti-fungal Waikialoids, Amoenamide B, Speramides, and Asperochramides; and (2) the monooxopiperazines that includes: the anti-parasitic Paraherquamides from *Penicillium* spp., the Asperparalines, Marcfortines, calmodulin-inhibiting Malbrancheamides, Chrysogenamide, Mangrovamides, Penioxalamine, Penicimutamides, and Asperversiamides.[1, 3, 4]

BA and **BB** represent the first isolated natural alkaloids comprising the bicyclo[2.2.2]diazaoctane core (Fig. 1a).[2] After we elucidated the correct absolute configuration of natural (+)-**BB** through total synthesis,[5, 6] it became evident that the biogenesis of **BA**/**BB** must accommodate assembly of the core tricyclic ring systems that are *pseudo*-enantiomeric. Several biogenetic hypotheses based on the pioneering proposal first suggested by Porter and Sammes in 1970[7] reasoned that the bicyclo[2.2.2]diazaoctane core arises *via* an intramolecular [4+2] *hetero*-Diels-Alder (IMDA) construction.[8, 9, 10, 11, 12, 13] Specifically (Fig. 1, Supplementary Fig. 1), a highly modified, reverse-prenylated indole (**1**, *e.g.*, Deoxybrevianamide E (**DE**)) undergoes a presumed indole 2,3-epoxidation either before or after the IMDA cyclization. Ring-opening of the epoxide **2** can form 3-hydroxyindolenines (**3**), which in some instances are stable (*e.g.*, Taichunamide A[14]) or, suffers a spontaneous semi-pinacol rearrangement to generate 3-*spiro*-ψ–indoxyls (**4**, *e.g.*, **BA**), or *spiro*-2-oxindoles (**5**, *e.g.*, Notoamide

A[15]) *via* an alternative ring-opening intermediate **6**.[1, 3, 4]

While the *spiro*-2-oxindoles are more frequently observed in the prenylated indole alkaloid family, only a small number of 3-*spiro*-ψ-indoxyl species have been isolated so far, and very rarely are natural *spiro*-2-oxindole species and 3-*spiro*-ψ-indoxyls co-produced by a single microbe.[16, 17] These co-metabolite profiles suggest that the semi-pinacol rearrangement might be differentially controlled in the partitioning of the putative indole-2,3-epoxides and implies a specific biocatalyst-controlled mechanism. Recently, the chemical synthesis of **BA**, the typical structure that contains the dioxopiperazine and 3-*spiro*-ψ−indoxyl moieties, has been accomplished and suggested a Diels-Alderase-free biosynthesis.[18] However, the biocatalytic details and the sequential timing for the putative indole oxidation, semi-pinacol rearrangement, and IMDA cycloaddition (Supplementary Fig. 1) remain unresolved experimentally due to lack of access to the key enzymes. Thus, we sought to solve these important mechanistic problems by elucidating the **BA** biosynthetic pathway.

Results

[Insert title of subsection here]

Initially, genome mining of a **BA** producing strain *P. brevicompactum* NRRL 864 (*Pb*) was conducted using the Notoamide nonribosomal peptide synthetase (NRPS) gene *notE* as a probe to search for its homolog responsible for assembling the cyclodipeptide Brevianamide F (**BF**).[3] A putative 16 kb **BA** biosynthetic gene cluster (*bvn*, GenBank accession number: MN401751) was revealed (Fig. 2a) that contains *bvnA* (NRPS), *bvnB* (flavin monooxygenase, FMO), *bvnC* (prenyltransferase, PT), and *bvnD* (P450 monooxygenase, P450), all of which have homologs in the (+)-/(-)-Notoamide A biosynthetic gene clusters[3]. The *bvnE* gene (465 bp) that encodes a putative isomerase shows low homology to Trt14, AusH and PrhC involved in meroterpenoid biosynthetic pathways.[19] Interestingly, the biosynthetic gene clusters of the *spiro*-2-oxindole containing Notoamides and Paraherquamides[3] lack a *bvnE* homolog, and further mining of these corresponding genomes failed to identify homologous genes. Thus, we surmised that BvnE might play an important role in 3-*spiro*-ψ-indoxyl formation.

In the *bvn* gene cluster, the bimodular NRPS encoded by *bvnA* is presumed to catalyze **BF** formation. This was confirmed by its heterologous expression in *Aspergillus oryzae* NSAR1 (*Ao*) (Supplementary Fig. 2). To investigate the function of *bvnB-E*, four individual single gene knockout (KO) strains of *Pb* were constructed. The resulting *Pb-bvnC*-KO strain accumulated **BF** (Fig. 2b) as the only product. The *Pb-bvnB*-KO and *Pb-bvnD*-KO strains accumulated **DE** and Brevianamide E (**BE**) (Fig. 2b), respectively. **BE** is proposed to be a rearranged shunt product resulting from initial 2,3-indole epoxidation of **DE** by BvnB FMO (Fig. 2f). Indeed, the recombinant *N*-His_6-tagged BvnB efficiently converted **DE** into **BE** *in vitro* (Fig. 2c) likely through a mechanism previously demonstrated for NotB[20] (a BvnB homolog with 62%/75% identity/similarity) in Notoamide biosynthesis. Since *Pb-bvnD*-KO did not produce a bicyclo[2.2.2]diazaoctane structure, we reasoned that BvnD is a key enzyme for the proposed IMDA reactions. When *bvnE* was deleted in *Pb*, five detectable substances were observed in addition to low levels of **BA** (Supplementary Table 1, Supplementary Fig. 3-4) and **BB** (Fig. 3a), all showing the same molecular weight of 365 Da (Supplementary Fig. 5). These include three previously unknown 3-hydroxyindolenine

derivatives **7**–**9** and the two reported *spiro*-2-oxindoles Brevianamide X (**BX**) and Brevianamide Y (**BY**). The planar structure of **7** was constructed based on 1D and 2D nuclear magnetic resonance (NMR) analyses (Supplementary Table 2, Supplementary Figs. 6-11): the key HMBC correlations of H_3-23/24 to C-2/19/22, H_2-10 to C-2/3/11/19, and H-4 to C-3 (Supplementary Fig. 10) readily built the hexatomic ring neighboring the indole base; the C-2=N double bond was deduced from the chemical shift of C-2 (189.29 *ppm*); and the *α*-configuration of 3-OH was determined from the NOESY analysis (Supplementary Fig. 11). The absolute configuration of **7** was determined by comparison of the experimental and computational ECD spectra (Supplementary Fig. 12). The structures of **BX** and **BY** were determined through high resolution mass spectrometry (HRMS) (Supplementary Fig. 5), NMR analyses (Supplementary Table 1, Supplementary Figs. 13-24), and comparison with the corresponding synthesized authentic standards (*see* Supplementary Information). Their absolute configurations were established by single-crystal X-ray diffraction (CCDC No. BX: 1973959, BY: 1973957; Supplementary Table 3, Supplementary Fig. 12). The ratio of **BA**:**BB**:**7**:**BX**:**BY** was determined to be 1:1:7:5:9 (Supplementary Table 4). Instability of **8** and **9** prevented direct structural determination of these isomers. Nonetheless, the observations that **8** and **9** quickly collapsed to **BY**/**BB** and **BX** (Supplementary Fig. 25), respectively, and their similar UV spectra to that of **7** suggested the structures of these two unstable metabolites being 3-hydroxyindolenines (Fig. 3c, Supplementary Fig. 26). To determine the structures of **8** and **9**, we chemically synthesized their hypothetical structures (*see* Supplementary Information, Supplementary Figs. 27-30). The matched UV spectra and retention times on HPLC, and the same decomposition behaviors of the synthetic standards to the isolated samples (Supplementary Fig. 31) confirmed their structures.

To validate the function of *bvn* genes and also to clarify the order of biosynthetic steps, we conducted heterologous expression with different gene combinations in *Ao*. As expected, **BF** was converted into **DE** by either *Ao-bvnC in vivo* (Fig. 2d) or purified BvnC *in vitro* in the presence of DMAPP and Mg^{2+} (Fig. 2e). Thus, PT BvnC is a Deoxybrevianamide E synthase as previously demonstrated for NotF.[21] *Ao-bvnCDE* produced **DE** exclusively in the feeding experiment, while *Ao-bvnBC* and *Ao-bvnBCE* both accumulated **BE** exclusively (Fig. 2d). These results indicate that the presumed indole epoxidation catalyzed by FMO BvnB occurs *prior to* the P450 BvnD-mediated step and preceding the BvnE-catalyzed step. Upon introduction of **BF** to the *Ao-bvnBCD* culture, five products with identical *m/z* 366 ($[M+H]^+$) were observed (Fig. 3b, Supplementary Fig. 5). Their relative abundance (**BA**:**BB**:**7**:**BX**:**BY** = 1:1:5:2:6) was qualitatively consistent with the observations in *Pb-bvnE*-KO (Fig. 3a, Supplementary Table 4) except that **8** and **9** were not detected probably due to their instability. Finally, when *bvnE* was incorporated, and the *Ao-bvnBCDE* strain grown in the presence of exogenous **BF**, we observed **BA** and **BB** in ~10:1 ratio (Fig. 3b, Supplementary Table 4), which is consistent with the product profile of wild-type *Pb* (*Pb*-WT) (Fig. 3a).

These results demonstrated that the metabolites generated through *Ao* biotransformations and individual *Pb* knockout mutants correlated directly with one another. The reaction sequence of each enzyme in the pathway can now be deduced as BvnA→BvnC→BvnB→BvnD→BvnE (Fig. 2f). Both systems showed a BvnE-dependent change of product profile, suggesting that BvnE might function to mediate formation of the 3-*spiro*-ψ-indoxyl species **10**, and directly impacts diastereo-outcome of the presumed IMDA reactions. With respect to BvnD activity, intensive attempts to produce this P450 enzyme in *E. coli* and *Saccharomyces cerevisiae* were unsuccessful, thus preventing direct functional analysis. Nonetheless, the results that *Ao-bvnBCD* transformed **BF** into multiple IMDA products (Fig. 3b) and that *Ao-bvnCDE* was unable to recognize **DE** as a substrate (Fig. 2d), and the principles for

P450 enzymes and Diels-Alder reactions together suggest that BvnD might oxidize a non-isolable intermediate **11** (derived from ring opening of the indole epoxide **12**) to **13**, thereby generating the diene moiety required for IMDA cyclization (Fig. 2f). In the absence of BvnD, compound **11** would collapse to **BE** via an energetically favored N-C ring closure (Supplementary Fig. 32).

Although we cannot exclude the possibility that BvnD might directly desaturate the N-C bond in the dioxopiperazine ring of **11**,[22] it is more likely that BvnD first catalyzes hydroxylation of **11** and then undergoes spontaneous dehydration/tautomerization to yield **13** (Fig. 2f). Regarding the position on **11** likely oxidized by BvnD, bond dissociation energy calculations (Supplementary Fig. 33) indicated that the most probable hydroxylation site is the tertiary C-H bond at C-11, which is supported by (1) FtmG, a BvnD homolog with 47%/64% protein sequence identity/similarity in the Fumitremorgin biosynthetic pathway, has been experimentally confirmed to catalyze hydroxylation of an analogous position;[22] and (2) a fungal dioxopiperazine structure Asperversiamide I was recently discovered to contain the C-11 hydroxylation, which might be installed by an unidentified BvnD homolog.[23]

[Insert title of subsection]

Based on the results of *Pb-bvnE*-KO and *Ao-bvnBCD* (Fig. 3), BvnE appeared to be a central enzyme for controlling the product profile in Brevianamide biogenesis. To assess this unique isomerase *in vitro*, the *N*-His_6-tagged BvnE was produced in *E. coli* BL21(DE3) and purified to homogeneity (Supplementary Fig. 34). Next, we sought to identify the potential natural substrate of BvnE from *Pb-bvnE*-KO. Compounds **7**, **8**, **9**, **BX**, **BY**, and **BE** were tested as substrates, but failed to be transformed (Supplementary Figs. 35-36). Thus, we hypothesized that **13** might be the native substrate of BvnE. Considering the inaccessibility of this unstable intermediate, we selected to chemoenzymatically synthesize **15** (*see* Supplementary Information), a stable analog of **13** (Fig. 4c) in order to block the dioxopiperazine nitrogen from N-C ring closure, and prevent formation of the unstable azadiene intermediate upon spontaneous dehydration. The mechanistic probe **15** was prepared through BvnB *in vitro* conversion of the chemically synthesized *N*-methyl-Deoxybrevianamide E (**14**) (Supplementary Figs. 37-45); and the absolute configuration of **15** was determined by single-crystal X-ray diffraction (CCDC No. 1973958, Supplementary Fig. 12). Interestingly, two minor products **16** and **17** were also generated from **14** along with the predominant product **15** (Fig. 4a). Structural determination indicated that **16** and **17** are 3-*spiro*-ψ-indoxyl and *spiro*-2-oxindole isomers of **15**, respectively (Supplementary Table 5, Supplementary Figs. 37, 46-57). Their absolute configurations were determined by comparison of their experimental and calculated ECD spectra (Supplementary Fig. 12), which were consistent with the structures arising from the semi-pinacol rearrangement of **15**. Moreover, when **15** was incubated with BvnE, it was completely converted into **16** (Fig. 4b). These results revealed that BvnE is a cofactor-independent pinacolase responsible for the selective formation of the 3-*spiro*-ψ-indoxyl sub-structure (in **16**) from the 3-hydroxy-pyrrole moiety (in **15**). Spontaneous conversion from **15** to **16** and **17** at room temperature could also occur slowly (Fig. 4c, Supplementary Fig. 58). Loss of stereocontrol of IMDA cycloaddition in terms of *top*/*bottom* (**7**/**9**/**BA**/**BX** *vs* **8**/**BY**/**BB)** and *anti*/*syn* selectivity **(7**/**8**/**BA**/**BB**/**BY** *vs* **9**/**BX)** in the absence of BvnE strongly suggests that these isomers are generated from non-enzymatic IMDA reactions. Moreover, the observed product profile (Fig. 3, Supplementary Table 6) is quantitatively consistent with the calculated product distribution (see below). With respect to the catalytic properties of BvnE (Supplementary Fig. 59), the apparent k_{cat} and K_m values of BvnE towards **15** were determined

to be 0.013 min^{-1} and 822 μM^{-1}, respectively, under the optimal pH (6.5) and temperature (30 °C). The low catalytic efficiency (k_{cat}/K_m = 1.58 × 10^{-5} min^{-1} μM^{-1}) was probably because **15** is not the native substrate.

As a key component in controlling product outcome in Brevianamide biosynthesis, we sought to determine how BvnE catalyzes formation of the 3-*spiro*-ψ-indoxyl species. BvnE is related to NTF2-like superfamily enzymes that have been studied in fungal meroterpenoid biogenesis.[19] We solved the crystal structure of BvnE at 1.8 Å resolution (Fig. 5a, Supplementary Table 7, PDB ID: 6U9I) by molecular replacement using PrhC (PDB ID: 5X9J) as a search model (Supplementary Fig. 60).[24] BvnE is a symmetric homodimer that adopts an α+β-barrel fold with the presumed active sites at the end of each barrel. This cavity has a hydrophobic interior and also contains several polar residues, which could be involved in the acid-base chemistry reported for this family of enzymes (Fig. 5a, Supplementary Fig. 61).

Docking of the presumed native substrate **13** (Fig. 5b, Supplementary Fig. 62a) helped reveal the BvnE active site. We identified Arg38, Tyr109, Tyr113 and Glu131 as candidates for site-directed mutagenesis and *in vitro* enzyme assays with **15**. In each case, mutation of these residues caused severely attenuated activity (Fig. 5c). All CD spectra of BvnE mutants matched wild-type protein (Fig. Supplementary 62b), indicating that these point mutations did not significantly impact protein folding. The electron density indicated that Arg38, Tyr113 and Glu131 adopt multiple conformations in the BvnE crystal lattice. Therefore, these residues were designated as flexible in molecular docking (Fig. Supplementary 62c). In the lowest energy output of the BvnE-**13** docking complex, the substrate reverse prenyl group packed into a hydrophobic pocket (Fig. Supplementary 62a), and Tyr109 and Tyr113 interacted with the 3–OH of **13** (Fig. 5b). Glu131 is positioned to interact with the indole nitrogen and the C-18 oxygen of **13**, suggesting its key role in the semi-pinacol rearrangement. (Fig. 5d). On the basis of these docking studies, we propose that the reaction mechanism of BvnE includes: (1) Glu131-mediated proton transfer to initiate the semi-pinacol rearrangement and to provide charge stabilization of the intermediate, and (2) hydrogen bond-assisted activation of the semi-pinacol rearrangement through Tyr109/Try113 (Fig. 5d). Arg38, which was essential for activity, does not directly interact with the docked ligands or active site residues. However, the structure reveals two ordered water molecules in a hydrogen bonding network between Arg38 and Glu131(Fig. Supplementary 62c), suggesting that it may assist in proton transfer by regenerating the carboxylate form of E131.

[Insert title of subsection]

Next, we used density functional theory and coupled cluster theory calculations (SMD-DLPNO-CCSD(T)//M06-2X-D3/6-31+G(d,p))[25] to evaluate the intermediate and transition state (TS) structures in the revised Brevianamide biosynthetic pathway (Supplementary Figs. 2f and 3c), and to explore innate regio- and stereochemical preferences associated with key steps (Fig. 6a). Accordingly, under *Pb-bvnE*-KO conditions, the IMDA reactions that transform **13** into **7**-**9** are favored. In the calculated mechanism, only two diastereomers of **7** (**8** and **9**) undergo a subsequent 1,2-alkyl shift to irreversibly generate **BY**/**BB** (from **8**), and **BX** (from **9**). Before the shifts that lead to ring system formation, an initial tautomerization that switches the position of the OH group between C3 and C2 proceeds quickly (Supplementary Fig. 63). The reason **7** fails to undergo subsequent transformation is likely due to the high energy required for the tautomerization process (35.5 kcal·mol-1 between **7** and its tautomer) (Supplementary Fig. 64). In the computed kinetic profile, the initial

irreversible IMDA (from **13** to **7**-**9**) and CH2-dioxopiperazine shift (from **13** to **10**) determine the selectivity of the process and their activation barriers are consistent with room-temperature reactivity over the course of minutes/hours. Considering that **BY** and **BX** are the major products obtained from **8** and **9**, respectively, the calculated results agree qualitatively with the experimental results: the two most favorable products are **7** and **BY**, followed by **BX**; and **BA** and **BB** are minor products (experimental ratio, **BY**:**7**:**BX**:**BA**:**BB** = 9:7:5:1:1, Supplementary Table 4).

The semi-pinacol rearrangement to form 3-spiro-ψ-indoxyl **10** is favorably exergonic and irreversible (ΔG -11.6 kcal·mol^{-1}). Competition between the two possible non-enzymatic semi-pinacol rearrangements (CH_2-dioxopiperazine *vs.* reverse-prenyl shifts) was found computationally to depend strongly on whether the reaction undergoes basic activation of the hydroxyl group or acidic activation of the imine group (Fig. 6b): whereas general/specific acid activation at nitrogen results in a buildup of positive charge in the migrating group in the TS, favoring 1,2-prenyl migration (ΔΔG‡ 8.8 kcal·mol^{-1}), basic activation of the hydroxyl group has the opposite effect, inverting the selectivity to favor migration of the dioxopiperazine-containing group (ΔΔG‡ 0.7 kcal·mol^{-1}). The contrast between regioselective biocatalytic conversion of **13** into **10** and the spontaneous conversion of **15** to **16**/**17** under acid-base conditions corroborates the involvement of hydrogen-bond acceptors Tyr113 or Tyr109 as a likely candidate for activation of the 3-hydroxyl group in BvnE (Fig. 5d, Supplementary Fig. 65) during this key step.

Next, we investigated distinct IMDA cyclizations from **10** and **13** (Fig. 6a). In each case, there are four possible stereochemical outcomes. The selectivity for *anti*- over *syn*-cycloadducts is controlled by the balance stabilizing intramolecular H-bonds and unfavorable steric interactions (Supplementary Fig. 66). Whereas *syn*-pathways from **10** are highly disfavored relative to *anti*-pathways, those from **13** form C−H···O interactions[26, 27], making them more competitive (Supplementary Fig. 67). In this regard, the levels of IMDA diastereoselectivity of **10** are exceptional, displaying high selectivity for the formation of **BA** over *pseudo*-enantantiomeric bicyclo[2.2.2]diazaoctane **BB** by 2 kcal·mol^{-1} due to an intramolecular N−H···O hydrogen bond, with a very large (*ca*. 6 kcal·mol^{-1}) preference for the two *anti*-configured products over their *syn*-diastereomers (Fig. 6a). The stereospecific conversion of **7** into **BA**, via a ring-contraction was found to be more challenging than the earlier 1,2-rearrangements (activation barrier of 28.2 kcal·mol^{-1}), however, this process is exergonic by 4 kcal·mol^{-1}. Accordingly, this ring-contraction can be accomplished under laboratory conditions by treating **7** with sodium hydroxide in water (Fig. 3c, Supplementary Fig. 68).

In conclusion, we have characterized and fully reconstituted **BA**/**BB** biosynthesis and identified the first cofactor-independent pinacolase BvnE as a key enzyme for diastereocontrol in the non-Diels-Alderase biogenesis of the Brevianamides. The [4+2] IMDA-derived dioxopiperazine bicyclo[2.2.2]diazaoctane core construction has also been demonstrated and the computational data support a spontaneous pericyclic reaction. Resolution of this non-Diels-Alderase mechanistic mystery of dioxopiperazine together with our recent characterization of the Diels-Alderase-mediated biogenesis of monooxopiperazines[28] highlight the diversified biosynthetic strategies deployed by fungi for creating structurally diverse *spiro*-cyclized indole alkaloids. Several important mechanistic questions nonetheless remain, including: 1) what are the mechanistic details of the BvnD-catalyzed two-electron oxidation required for azadiene formation to enable the IMDA, and 2) what, if any, biogenetic relationships exist between Brevianamides and other dioxopiperazine families comprised of the bicyclo[2.2.2]diazaoctane system, such as (+)/(-)-Notoamide A whose producer genomes lack *bvnE* homologs?

Methods

Data Availability

Acknowledgements

This work was supported by the National Key Research and Development Program (2019YFA0905100 and 2019YFA0706900), the National Natural Science Foundation of China (21472204 and 31872729 to S.L. and 31800041 to L.D.), the National Institutes of Health R01 CA070375 (to R.M.W. and D.H.S.), R35 GM118101, the Hans W. Vahlteich Professorship (to D.H.S.), the Shandong Provincial Natural Science Foundation (ZR2019ZD22 to S.L. and ZR201807060986 to L.D.), the National Postdoctoral Innovative Talents Support Program (BX20180325 to L.D.), China Postdoctoral Science Foundation (2019M652500 to L.D.), and funding from NSF grant CHE-0840456 (for X-ray instrumentation). GM/CA@APS is supported by the National Institutes of Health, National Institute of General Medical Sciences (AGM-12006) and National Cancer Institute (ACB-12002). We also thank Professor Janet L. Smith from University of Michigan for her assistance with the structure determination of BvnE. R.S.P. acknowledges computational resources from the RMACC Summit supercomputer supported by the National Science Foundation (ACI-1532235 and ACI-1532236), the University of Colorado Boulder and Colorado State University, and the Extreme Science and Engineering Discovery Environment (XSEDE) through allocation TG-CHE180056. XSEDE is supported by the National Science Foundation (ACI-1548562). The authors thank Ms. Xiaoju Li and Ms. Haiyan Sui from The State Key Laboratory of Microbial Technology, Shandong University for the assistance in X-ray single crystal diffractometer.

Author Contributions Y.Y., L.D., R.M.W., D.H.S., S.L. contributed to the experimental design. Y.Y., L.D., W.Z., and F.Q. performed molecular cloning, fungal genetics and compounds purification. Y.Y., L.D. and X.Z. performed structural assignment (NMR analysis). Y.Y., L.D., S.A.N., A.E.F. and M.L.A. performed molecular cloning, protein expression and purification. Y.Y., L.D. performed enzymatic assays and LC/MS and HPLC analysis. S.A.N. and M.L.A. carried out all crystallographic experiments, structural analysis. Y.Y. performed structure-based site-directed mutagenesis. W.Z performed genome mining of the gene cluster. M.M., N.C., V.V.S. and S.M. synthesized and validated the compounds described in this study. J.V.A. and R.S.P. performed DFT calculations. A.M. and H.O. supplied the heterologous expression system. H.K. and S.T. performed ECD measurement and calculations. Y.Y., L.D., S.A.N., R.S.P., R.M.W., D.H.S. and S.L. analyzed the data and prepared the manuscript.

Competing interests

References

1. Klas KR *et al.* Structural and stereochemical diversity in prenylated indole alkaloids containing the bicyclo 2.2.2 diazaoctane ring system from marine and terrestrial. *Nat. Prod. Rep.* **35** 532-558 (2018).

2. Birch AJ, Wright JJ. The brevianamides: a new class of fungal alkaloid. *J. Chem. Soc. D* 1969(12)**:** 644b-645.
3. Li S, Srinivasan K, Hong T, Yu F, Finefield JM, Sunderhaus JD, *et al.* Comparative analysis of the biosynthetic systems for fungal bicyclo 2.2.2 diazaoctane indole alkaloids: the (+)/(-)-notoamide, paraherquamide and malbrancheamide pathways. *MedChemComm* 2012, **3**(8)**:** 987-996.
4. Finefield JM, Frisvad JC, Sherman DH, Williams RM. Fungal origins of the bicyclo 2.2.2 diazaoctane ring system of prenylated indole alkaloids. *J. Nat. Prod.* 2012, **75**(4)**:** 812-833.
5. Williams RM, Glinka T, Kwast E. Facial selectivity of the intramolecular SN2' cyclization: stereocontrolled total synthesis of brevianamide B. *J. Am. Chem. Soc.* 1988, **110**(17)**:** 5927-5929.
6. Williams RM, Kwast E, Coffman H, Glinka T. Remarkable, enantio-divergent biogenesis of brevianamide A and B. *J. Am. Chem. Soc.* 1989, **111**(8)**:** 3064-3065.
7. Porter AEA, Sammes PG. A Diels-Alder reaction of possible biosynthetic importance. *J. Chem. Soc. D* 1970(17)**:** 1103a.
8. Sanzcervera JF, Glinka T, Williams RM. Biosynthesis of the brevianamides: quest for a biosynthetic Diels-Alder cyclization. *J. Am. Chem. Soc.* 1993, **115**(1)**:** 347-348.
9. Sanzcervera JF, Glinka T, Williams RM. Biosynthesis of brevianamides A and B: in search of the biosynthetic Diels-Alder construction. *Tetrahedron* 1993, **49**(38)**:** 8471-8482.
10. Williams RM, Sanz-Cervera JF, Sancenon F, Marco JA, Halligan K. Biomimetic Diels-Alder cyclizations for the construction of the brevianamide, paraherquamide sclerotamide, and VM55599 ring systems. *J. Am. Chem. Soc.* 1998, **120**(5)**:** 1090-1091.
11. Adams LA, Valente MWN, Williams RM. A concise synthesis of d,l-brevianamide B via a biomimetically-inspired IMDA construction. *Tetrahedron* 2006, **62**(22)**:** 5195-5200.
12. Williams RM, Cox RJ. Paraherquamides, brevianamides, and asperparalines: laboratory synthesis and biosynthesis. An interim report. *Acc. Chem. Res.* 2003, **36**(2)**:** 127-139.
13. Stocking EM, Williams RM. Chemistry and biology of biosynthetic Diels-Alder reactions. *Angew. Chem. Int. Ed.* 2003, **42**(27)**:** 3078-3115.
14. Li F, Zhang Z, Zhang G, Che Q, Zhu T, Gu Q, *et al.* Determination of taichunamide H and structural revision of taichunamide A. *Org. Lett.* 2018, **20**(4)**:** 1138-1141.
15. Greshock TJ, Grubbs AW, Jiao P, Wicklow DT, Gloer JB, Williams RM. Isolation, structure elucidation, and biomimetic total synthesis of versicolamide B, and the isolation of antipodal (-)-stephacidin A and (+)-notoamide B from *Aspergillus versicolor* NRRL 35600. *Angew. Chem. Int. Ed.* 2008, **47**(19)**:** 3573-3577.
16. Kai A, Kato H, Sherman DH, Williams RM, Tsukamoto S. Isolation of a new indoxyl alkaloid, Amoenamide B, from *Aspergillus amoenus* NRRL 35600: biosynthetic implications and correction of the structure of Speramide B. *Tetrahedron Lett.* 2018, **59**(48)**:** 4236-4240.
17. Xu X, Zhang X, Nong X, Wang J, Qi S. Brevianamides and mycophenolic acid derivatives from the deep-sea-derived fungus *Penicillium brevicompactum* DFFSCS025. *Mar. Drugs* 2017, **15**(2).
18. Godfrey RC, Green NJ, Nichol GS, Lawrence AL. Chemical synthesis of (+)-brevianamide A supports a Diels–Alderase-free biosynthesis. 2019. Doi:10.26434/chemrxiv.8224148.v1.
19. Mori T, Iwabuchi T, Hoshino S, Wang H, Matsuda Y, Abe I. Molecular basis for the unusual ring reconstruction in fungal meroterpenoid biogenesis. *Nat. Chem. Biol.* 2017, **13**(10)**:** 1066-1073.
20. Li S, Finefield JM, Sunderhaus JD, McAfoos TJ, Williams RM, Sherman DH. Biochemical characterization of

NotB as an FAD-dependent oxidase in the biosynthesis of notoamide indole alkaloids. *J. Am. Chem. Soc.* 2012, **134**(2)**:** 788-791.

21. Ding Y, de Wet JR, Cavalcoli J, Li S, Greshock TJ, Miller KA, *et al.* Genome-based characterization of two prenylation steps in the assembly of the stephacidin and notoamide anticancer agents in a marine-derived *Aspergillus* sp. *J. Am. Chem. Soc.* 2010, **132**(36)**:** 12733-12740.
22. Kato N, Suzuki H, Takagi H, Asami Y, Kakeya H, Uramoto M, *et al.* Identification of cytochrome P450s required for fumitremorgin biosynthesis in *Aspergillus fumigatus*. *ChemBioChem* 2009, **10**(5)**:** 920-928.
23. Li H, Xu D, Sun W, Yang B, Li F, Liu M, *et al.* HPLC-DAD-Directed Isolation of Linearly Fused Prenylated Indole Alkaloids from a Soil-Derived Aspergillus versicolor. *J. Nat. Prod.* 2019, **82**(8)**:** 2181-2188.
24. Matsuda Y, Iwabuchi T, Fujimoto T, Awakawa T, Nakashima Y, Mori T, *et al.* Discovery of key dioxygenases that diverged the paraherquonin and acetoxydehydroaustin pathways in *Penicillium brasilianum*. *J. Am. Chem. Soc.* 2016, **138**(38)**:** 12671-12677.
25. Quantum chemical calculations were performed using Gaussian 16, rev B.01 and Orca 4.1.2. For a full description of computational methods and references see the Supporting Information.
26. Sutor DJ. The C–H… O Hydrogen Bond in Crystals. *Nature* 1962, **195**(4836)**:** 68-69.
27. Schwalbe CH. June Sutor and the C–H ⋯ O hydrogen bonding controversy. *Crystallography Reviews* 2012, **18**(3)**:** 191-206.
28. Dan Q, Newmister SA, Klas KR, Fraley AE, McAfoos TJ, Somoza AD, *et al.* Fungal indole alkaloid biogenesis through evolution of a bifunctional reductase/Diels–Alderase. *Nat. Chem.* 2019, **11**(11)**:** 972-980.

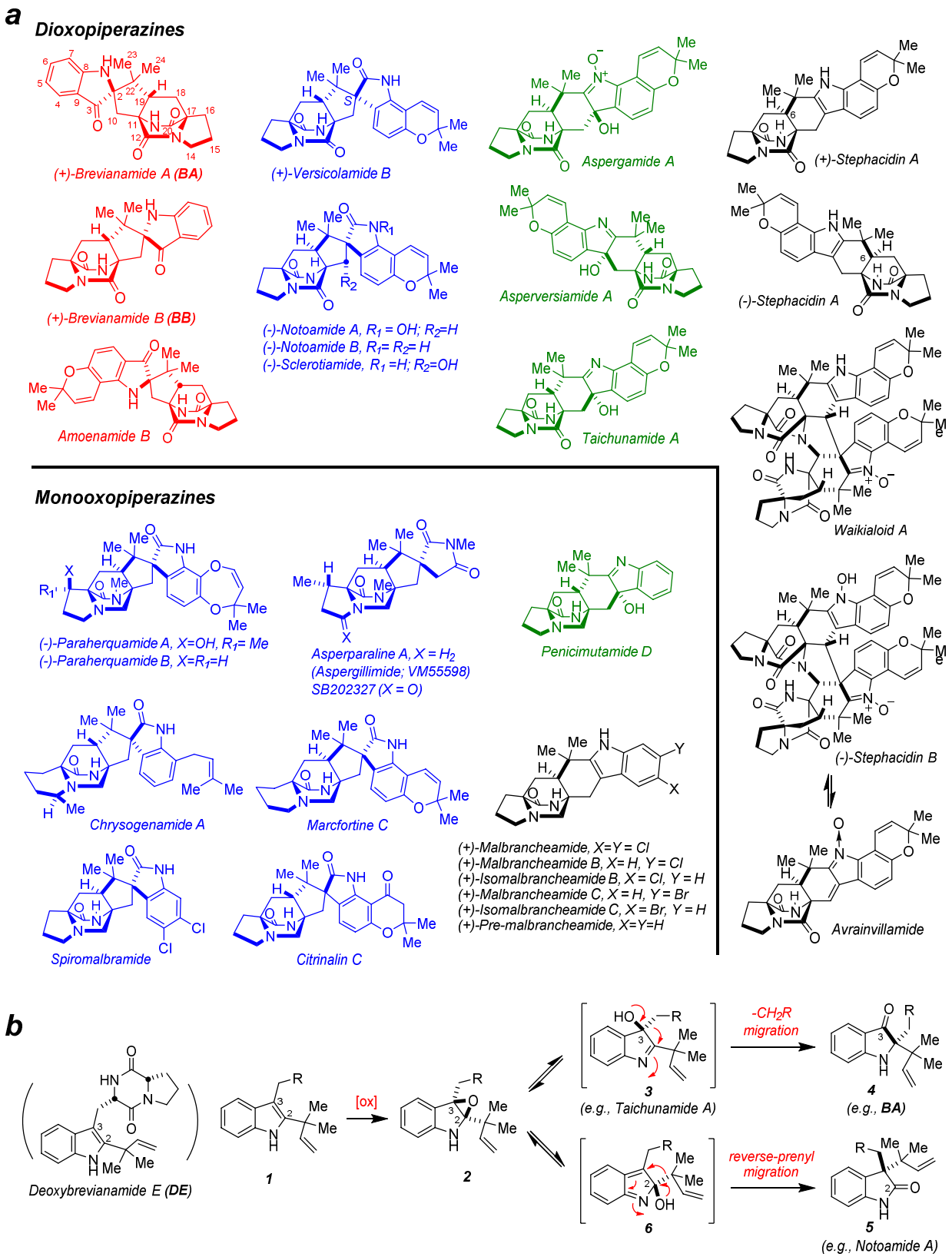

Fig. 1 Representative bicyclo[2.2.2]indole alkaloids (**a**) and related semi-pinacol rearrangements of indole-2,3-epoxide systems (**b**). Disparate fates of indole-2,3-epoxide moieties (**2**) and semi-pinacol rearrangements leading to indoxyls (**4**), oxindoles (**5**), and stable 3-hydroxyindolenines (**3**). Compounds with 3-*spiro*-ψ–indoxyls, *spiro*-2-oxindoles and 3-hydroxyindolenines are presented in red, blue and green, respectively.

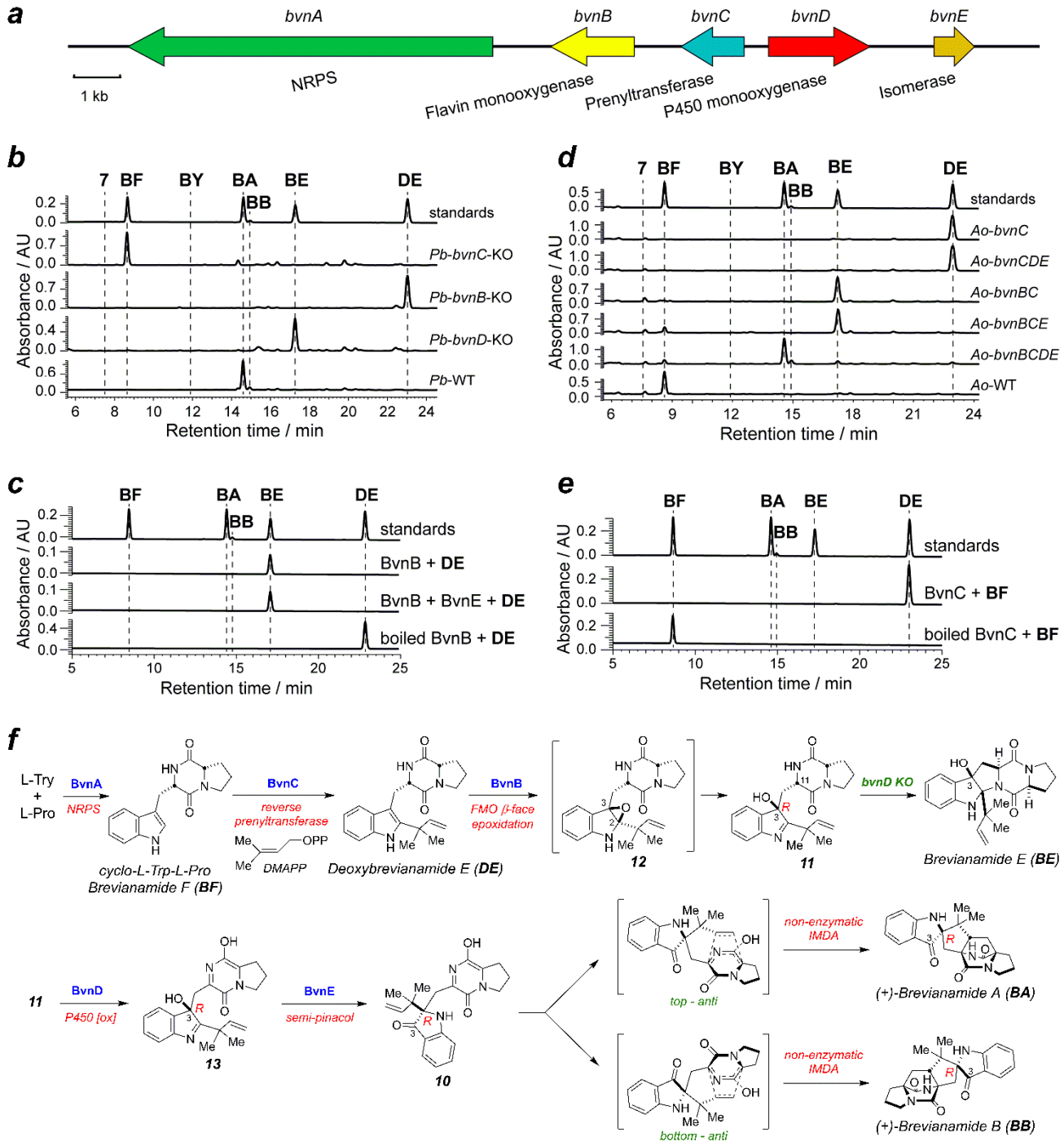

Fig. 2 The Brevianamide biosynthetic gene cluster (*bvn*), HPLC analyses (230 nm), and the proposed biosynthetic pathway for Brevianamides A and B (BA and BB). a, The *bvn* gene cluster from *Penicillium brevicompactum NRRL 864* (*Pb*); **b.** HPLC analysis of *Pb* KO mutants. **c**, HPLC analysis of the *in vitro* assays of BvnB and BvnE. **d**, HPLC analysis of the Brevianamide F (**BF**) feeding experiments with recombinant *Aspergillus oryzae* M-2-3 (*Ao*) strains expressing different *bvn* gene(s). **e**, HPLC analysis of *in vitro* assays using BvnC. **f**. Revised biosynthetic pathway for **BA** and **BB**.

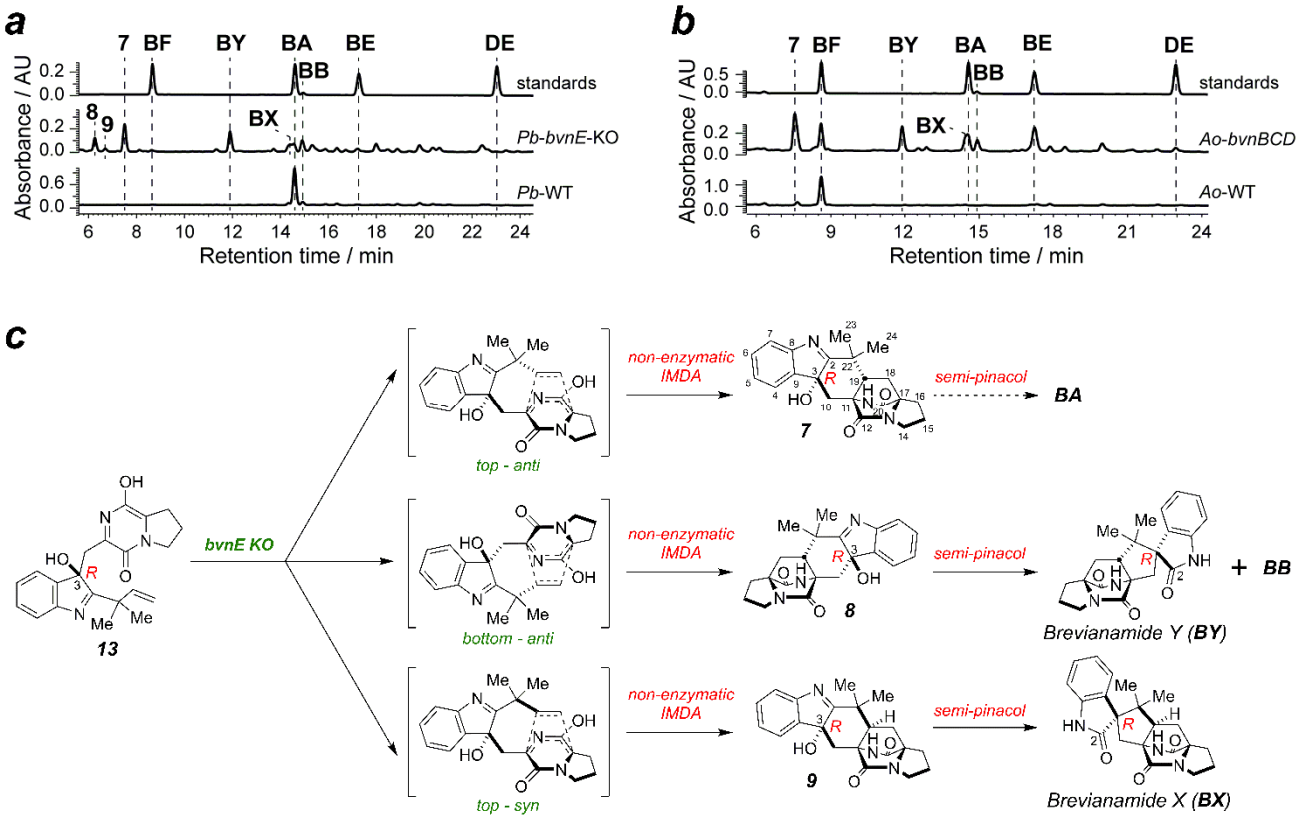

Fig. 3 HPLC analyses (230 nm) of *Pb bvnE* KO mutant (a) and the *Ao-bvnBCD mutant* (b), and the putative spontaneous transformations (c).

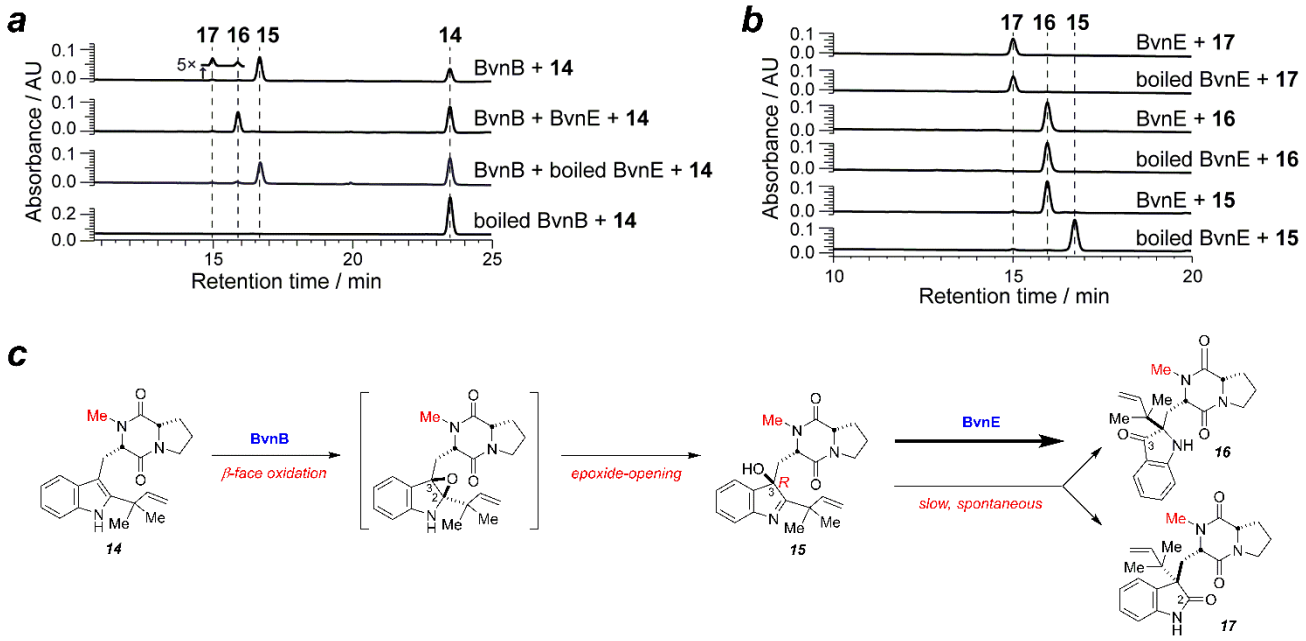

Fig. 4 HPLC analyses (230 nm) of the *in vitro* assays of BvnB/BvnE (a) and BvnE (b) with the *N*-methylated substrates and the corresponding reaction scheme (c).

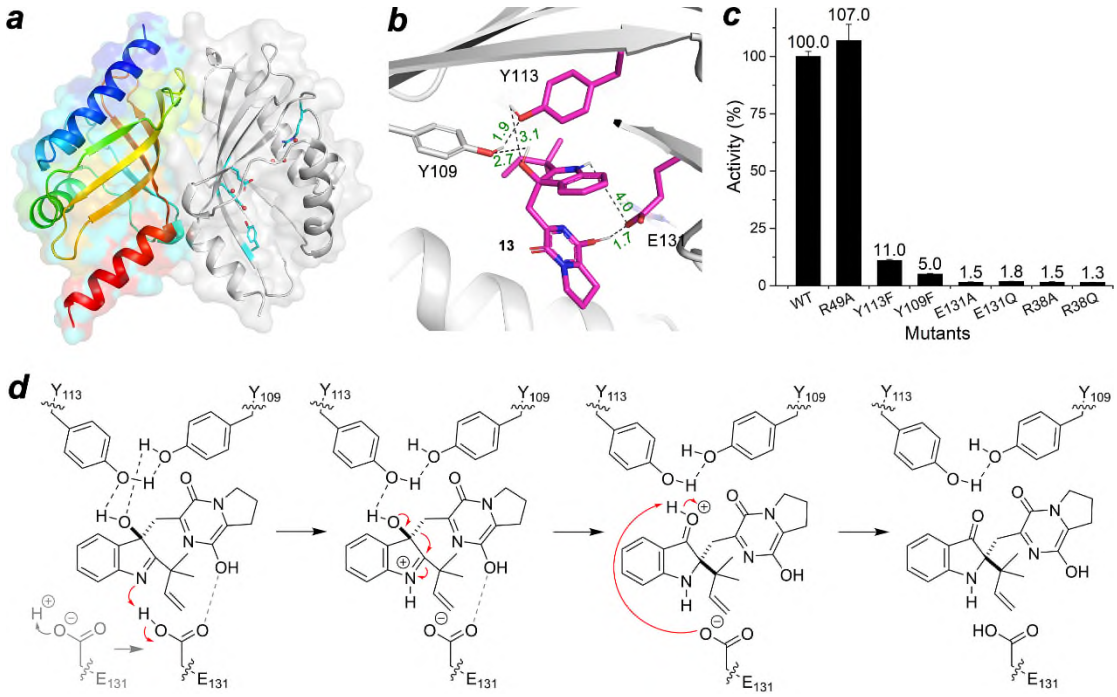

Fig. 5 BvnE crystal structure, docking and the proposed reaction mechanism. a, Structure overview of BvnE: left chain shown in rainbow spectrum from *N*-terminus (blue) to *C*-terminus (red); the right chain in grey cartoon with putative catalytic acid-basic residues (cyan) and water molecules in the active site (red spheres). **b**, BvnE-**13** complex with key residues and hydrogen bonding shown; **c**, Site-directed mutagenesis results; **d**, The proposed BvnE reaction mechanism for isomerization of **13**. Glu131-mediated proton transfer could be assisted by Arg38, which interacts with Glu131 via an ordered water network (Supplementary Fig. 62c). Indirect deprotonation of the oxonium intermediate via bound solvent molecules rather than a direct interaction with Glu131 cannot be excluded.

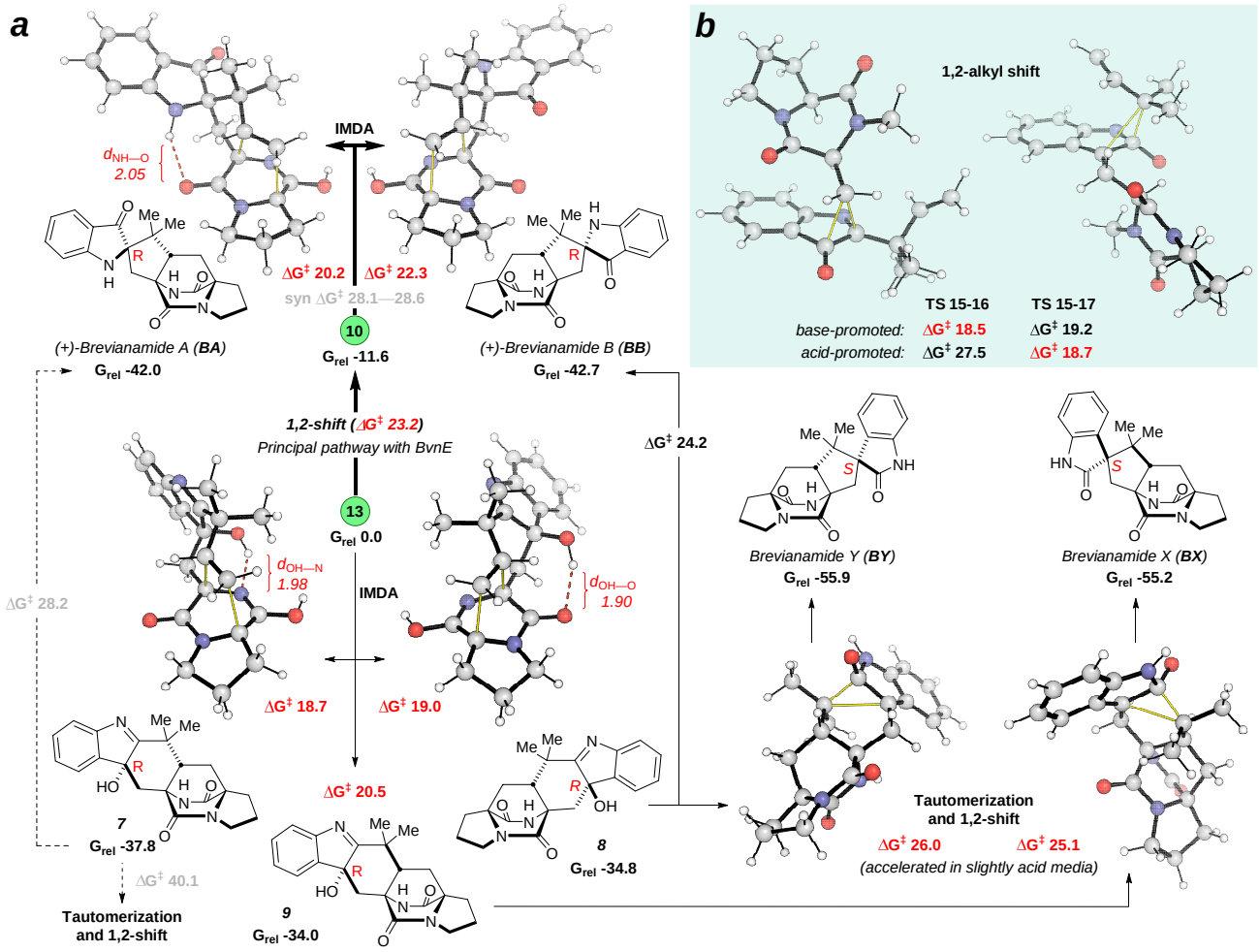

Fig. 6 Quantum chemical calculation results. a, *anti*-Selective IMDA transition structures and products accessible from intermediates **13** and **10**; **b**, 1,2-alkyl shift (semi-pinacol) transition structures for the migration of CH_2-dioxopiperazine (LHS) and reverse-prenyl (RHS) groups. Computed Gibbs energies are in kcal/mol and highlighted distances in Å. Normal lines follow the major pathways obtained under *Pb-bvnE*-KO conditions. Pathways in bold correspond to the major reactivity obtained when using BvnE (switch in reactivity). Dashed lines represent pathways with prohibitively high activation energies under the reaction conditions.